

# Higher forbidden unique $\beta^-$ decay transitions and shell-model interpretation

Archana Saxena<sup>1</sup> and Praveen C. Srivastava<sup>1,\*</sup>

<sup>1</sup>*Department of Physics, Indian Institute of Technology Roorkee, Roorkee 247667, India*

In the present work, we have predicted the half-lives for the  $\beta^-$  decay for higher forbidden unique transitions in the mass range of nuclei from  $A = 40$ -138. For these transitions, the experimental data for half-lives are not available except for a few cases. The calculations for half-lives are performed within the framework of the nuclear shell model (SM). We have used the effective interactions *sdp*fmu, *gxp*f1a, *gwb*xg, G-matrix, *snet*, *sn100pn*, and *jj56pnb* to perform the SM calculations in different mass regions. A comprehensive discussion has been made between the SM predicted half-lives and the scaled half-lives from proton-neutron quasiparticle random-phase approximation (pnQRPA). The results of the present study will be useful to plan new experiments to measure half-lives for these higher forbidden unique  $\beta^-$  transitions.

## I. INTRODUCTION

The nuclear  $\beta$ -decay, also known as the weak nuclear processes occurring inside the nuclei, is a powerful tool for exploring the structure and properties of atomic nuclei. It plays an important role in subatomic physics and astrophysics [1–10]. To study the  $\beta$ -decay, we need a theoretical model that can explain the properties of the nuclei. In the present work, we use the nuclear shell model (SM) to calculate the matrix elements involved in beta decay for higher forbidden unique transitions. The decay rates depend on the precisely calculated wave functions of parent and daughter nuclei involved in nuclear matrix elements (NMEs) [11].

The transitions in the  $\beta$ -decay can be categorized into two types, allowed and forbidden, based on the orbital angular momentum ( $l$ ) of the emitted leptons. When  $l = 0$ , it is categorized as allowed, while  $l > 0$  leads to forbidden transitions. Allowed transitions are characterized by a change in total angular momentum  $\Delta J = 0, \pm 1$  and no change in parity ( $\Delta\pi = +1$ ). The forbidden transitions are further categorized as forbidden non-unique (FNU) and forbidden unique (FU). For the  $K$ th-FNU transition,  $\Delta J = K$  (In case of  $K=1$ ,  $\Delta J = 0, 1$ ), where  $K$  is the order of forbiddenness and parity changes in the odd-forbidden and remains same in the even-forbidden decays according to  $\Delta\pi = (-1)^K$ . Basically, forbidden unique decays are a special case of forbidden non unique (FNU) decays. In the  $K$ th FU transition,  $\Delta J = K + 1$ , here, the angular momentum change between the initial and final nuclear states is maximal and parity follows the same as in FNU decays. Consequently, the decay rate and the shape factor are significantly simplified as the contribution of only one matrix element [12].

The majority of  $\beta$ -decay transitions observed in nature are of the allowed type and a few with a low order of ' $K$ '. However, recent research has focused on finding rare beta decays that have longer half-lives. These transitions are hindered by low  $Q$  value or high order of ' $K$ '. The theoretical formalism of nuclear beta decay is explained in the

book by Behrens and Bühring [13]. With advancements in measurement technology, the study of higher forbidden beta decays became interesting. Recently, half-lives for 148 forbidden unique beta transitions, including 2nd, 3rd, 4th, 5th, 6th, and 7th orders, have been predicted using the proton-neutron quasiparticle random-phase approximation (pnQRPA) model by Kostensalo and Suhonen [14]. The experimental half-lives for these higher forbidden unique transitions are not yet available.

The forbidden unique decays exhibit a straightforward dependence on the weak axial-vector coupling constant  $g_A$  ( $t_{1/2} \propto g_A^{-2}$ ). For bare nucleons, the value  $g_A = 1.27$  is extracted from the partially conserved axial-vector current hypothesis (PCAC) but this value is affected inside the nuclear matter due to nuclear medium effects or nuclear many-body effects and a quenching is needed to reproduce the experimental data. So, the role of  $g_A$  is important to calculate half-lives more precisely. There are few methods available to study the quenching in  $g_A$  values in higher forbidden unique  $\beta$ -decay. Previously, the effective value of  $g_A$  has been investigated through a half-life comparison method, where predicted and experimental values are compared across various  $g_A$  values [15–17]. This approach can be used to find out the quenching once experimental data becomes accessible. The spectrum-shape method (SSM) is the popular one to study the quenching in which the shapes of calculated and experimental electron spectra are compared [17–19]. In the present manuscript, we have done a systematic SM study for the higher forbidden unique  $\beta^-$  transitions to test the predictive power of our computed nuclear wave functions in the mass region  $A = 40$ -138.

The present manuscript is structured into the following sections. The section II is divided into two subsections: subsection II A explains the theoretical formalism used to calculate the shape factor, nuclear matrix elements (NMEs), and half-lives, while subsection II B reported the shell model Hamiltonian employed. Section III presents the SM results for half-lives of higher FU  $\beta^-$  decay transitions. Finally, we conclude the manuscript in Section IV.

\* praveen.srivastava@ph.iitr.ac.in

## II. THEORETICAL FRAMEWORK

### A. Formalism

In the present work, we have calculated the partial half-lives for the forbidden unique  $\beta^-$  transitions. The generalized theoretical formalism of nuclear  $\beta$ -decay is available in Refs [20, 21]. For allowed and forbidden types of  $\beta$ -decay, the detailed formalism is given in the books by Behrens and Bühring [13] and by Schopper [22]. The formalism of nuclear  $\beta$ -decay theory is based on the impulse approximation which says that the decaying nucleon doesn't interact with the other nucleons around it at the moment of decay. However, before and after the decay, it interacts with these nucleons strongly. This simplified approach helps in understanding and calculating both allowed and forbidden  $\beta$ -decay processes.

The expression for calculating the partial half-life is given as [13, 20]

$$t_{1/2} = \frac{\kappa}{\bar{C}}, \quad (1)$$

where  $\kappa$  is a constant and value is given as [23]

$$\kappa = \frac{2\pi^3 \hbar^7 \ln(2)}{m_e^5 c^4 (G_F \cos\theta_C)^2} = 6289 \text{ s}, \quad (2)$$

where,  $G_F$  is the Fermi constant and  $\theta_C$  is the Cabibbo angle. The  $\bar{C}$  is the dimensionless integrated shape function and can be calculated as

$$\bar{C} = \int_1^{w_0} C(w_e) p w_e (w_0 - w_e)^2 F_0(Z, w_e) dw_e. \quad (3)$$

In the above expression the usual dimensionless kinematics quantities divided by the electron rest mass are used as  $w_0 = W_0/m_e c^2$ ,  $w_e = W_e/m_e c^2$ , and  $p = p_e c/m_e c^2 = \sqrt{(w_e^2 - 1)}$ . The  $w_0$  is the endpoint energy,  $w_e$  and  $p_e$  are the total energy and momentum of emitted electrons, respectively. The term  $F_0(Z, w_e)$  is the Fermi function, and  $Z$  is the atomic number of the daughter nucleus. The  $C(w_e)$  is the shape factor that contains information about the nuclear structure.

The general form of shape factor  $C(w_e)$  is given as:

$$C(w_e) = \sum_{k_e, k_\nu, K} \lambda_{k_e} \left[ M_K(k_e, k_\nu)^2 + m_K(k_e, k_\nu)^2 - \frac{2\gamma_{k_e}}{k_e w_e} M_K(k_e, k_\nu) m_K(k_e, k_\nu) \right], \quad (4)$$

where,  $k_e$  and  $k_\nu$  ( $= 1, 2, 3, \dots$ ) are positive integers and associated with the partial-wave expansion of the leptonic wave functions, and  $K$  denotes the order of forbiddenness of the  $\beta$  decay. The terms  $M_K(k_e, k_\nu)$  and  $m_K(k_e, k_\nu)$  can be expressed in terms of different NMEs and other kinematic factors [13, 20]. Here,

$\gamma_{k_e} = \sqrt{k_e^2 - (\alpha Z)^2}$  and  $y = (\alpha Z w_e / p_e c)$  are the auxiliary quantities, and  $\alpha = 1/137$  is the fine structure constant and the term  $\lambda_{k_e} = F_{k_e-1}(Z, w_e) / F_0(Z, w_e)$ , is the Coulomb function, in which  $F_{k_e-1}(Z, w_e)$  is the generalized Fermi function [20, 21, 24] which can be calculated using formula

$$F_{k_e-1}(Z, w_e) = 4^{k_e-1} (2k_e) (k_e + \gamma_{k_e}) [(2k_e - 1)!!]^2 e^{\pi y} \times \left( \frac{2p_e R}{\hbar} \right)^{2(\gamma_{k_e} - k_e)} \left( \frac{|\Gamma(\gamma_{k_e} + iy)|}{\Gamma(1 + 2\gamma_{k_e})} \right)^2. \quad (5)$$

NMEs contain all the information about nuclear-structure and can be expressed as

$$\begin{aligned} & \text{V/A } \mathcal{M}_{KLS}^{(N)}(pn)(k_e, m, n, \rho) \\ &= \frac{\sqrt{4\pi}}{\hat{J}_i} \sum_{pn} \text{V/A } m_{KLS}^{(N)}(pn)(k_e, m, n, \rho) (\Psi_f || [c_p^\dagger \tilde{c}_n]_K || \Psi_i). \end{aligned} \quad (6)$$

Here, summation runs over the proton (p) and neutron (n) single particle states. The functions  $\text{V/A } m_{KLS}^{(N)}(pn)(k_e, m, n, \rho)$  are the single particle matrix elements (SPMEs), they do not depend on the nuclear models. The terms  $(\Psi_f || [c_p^\dagger \tilde{c}_n]_K || \Psi_i)$  are the one-body transition densities (OBTDs) between the initial ( $\Psi_i$ ) and final ( $\Psi_f$ ) nuclear states and these are model-dependent. In the present work, the SPMEs use harmonic oscillator wave functions [20, 21]. The OBTDs are calculated using nuclear shell model codes KSHHELL [25] and NUSHELLX [26]. We have also included here the next-to-leading-order (NLO) corrections to the shape factor which increase the number of NMEs (full details about the NLO corrections are given in Refs. [19, 20]).

### B. Shell-Model Hamiltonian

We have performed calculations within the framework of shell-model. The nuclear shell-model Hamiltonian can be written in terms of single particle energies and two nucleon interactions as

$$H = T + V = \sum_{\alpha} \epsilon_{\alpha} c_{\alpha}^{\dagger} c_{\alpha} + \frac{1}{4} \sum_{\alpha\beta\gamma\delta} v_{\alpha\beta\gamma\delta} c_{\alpha}^{\dagger} c_{\beta}^{\dagger} c_{\delta} c_{\gamma}, \quad (7)$$

where  $\alpha = \{n, l, j, t\}$  represents a single-particle state and  $\epsilon_{\alpha}$  is the single particle energy of state  $\alpha$  and  $c_{\alpha}^{\dagger}$  and  $c_{\alpha}$  are the fermion pair creation and annihilation operators. The term  $v_{\alpha\beta\gamma\delta} = \langle \alpha\beta | V | \gamma\delta \rangle$  represents the antisymmetrized two-body matrix element (TBME).

We have taken different effective interactions for different model spaces for nuclei ranging from mass  $A = 40 - 138$ . The effective interactions sdpf-mu [27], gxp1a [28], gwbox [29, 30], G-matrix [31], snet [32, 33], sn100pn [34, 35] and jj56pnb [36, 37] are used for the calculations and shown in last column of Tables I-II B.

In the case of sd<sub>pf</sub>-mu effective interaction we have used full sd<sub>pf</sub> model space with  $^{16}\text{O}$  as a core. The valence model space has the orbitals  $1d_{5/2}$ ,  $2s_{1/2}$ ,  $1d_{3/2}$ ,  $1f_{7/2}$ ,  $2p_{3/2}$ ,  $1f_{5/2}$  and  $2p_{1/2}$ . For the generation of a negative parity state in  $^{40}\text{K}$ , we have used a truncation of 1p-1h excitation from *sd* to *pf* shell. Here, we are exciting only one particle either proton or neutron, while 2p-2h calculations have been done for  $^{40}\text{Ca}$  case.

We have used gxpfla effective interaction for nuclei having mass range from  $A = 40 - 62$  and the calculations have been done without truncation in full *pf* model space and  $^{40}\text{Ca}$  is considered as a core. Here, the orbitals for valence protons and neutrons are  $1f_{7/2}$ ,  $2p_{3/2}$ ,  $1f_{5/2}$ ,  $2p_{1/2}$  with single particle energies (SPEs) (in MeV) are  $-8.6240$ ,  $-5.6793$ ,  $-1.3829$ ,  $-4.1370$ .

The model space of gwboxg effective interaction consists of  $1f_{5/2}$ ,  $2p_{3/2}$ ,  $2p_{1/2}$ ,  $1g_{9/2}$  proton orbitals and  $2p_{1/2}$ ,  $1g_{9/2}$ ,  $1g_{7/2}$ ,  $2d_{5/2}$ ,  $2d_{3/2}$ , and  $3s_{1/2}$  neutron orbitals and SPEs (in MeV) used in this interaction are  $-5.322$ ,  $-6.144$ ,  $-3.941$ ,  $-1.250$ , for the proton orbitals, and  $-0.696$ ,  $-2.597$ ,  $+5.159$ ,  $+1.830$ ,  $+4.261$ ,  $+1.741$  for the neutron orbitals, respectively using  $^{68}\text{Ni}$  as a core. This effective interaction is prepared with different interactions and the original 974 two-body matrix elements (TBMEs) are obtained from the bare G-matrix of the H7B potential [H7B] [38], for more details, see Refs [39–41]. For  $A = 84 - 92$  we apply 1p-1h truncation across  $N = 50$  shell, and from mass  $A=94$  to 104 we completely filled  $1g_{9/2}$  orbital and open all four neutron orbitals above  $N = 50$ .

Corresponding to G-matrix interaction, the model space of the present study consists of two proton orbitals  $2p_{1/2}$  and  $1g_{9/2}$  with SPEs (in MeV) are  $0.000$ ,  $+0.9000$  and five neutron orbitals  $2d_{5/2}$ ,  $3s_{1/2}$ ,  $2d_{3/2}$ ,  $1g_{7/2}$ , and  $1h_{11/2}$  with SPEs are  $0.000$ ,  $+1.2600$ ,  $+2.6300$ ,  $+2.230$ ,  $+3.500$  respectively. Here,  $^{88}\text{Sr}$  is taken as inert core and we have not employed any truncation in the present calculations. The realistic effective interaction obtained by the G-matrix approach, which was constructed by the effective microscopic interaction derived from a charge-symmetry breaking nucleon-nucleon potential [42] with further modifications in the monopole part and was used in Ref. [31].

The snet effective interaction consists of 17 orbitals, eight are proton orbitals and nine are neutron orbitals.

In the calculations using snet effective interaction, we have put a minimum of 8-10 protons in  $1g_{9/2}$  orbital and a maximum of 2 protons in  $1g_{7/2}$  orbital, while neutrons are occupying the  $1g_{7/2}$ ,  $2d_{5/2}$ ,  $2d_{3/2}$ ,  $3s_{1/2}$  and  $1h_{11/2}$  orbitals. Further, for computational reasons, we have restricted a minimum of 2-6 neutrons in the  $1h_{11/2}$  orbital from  $A=114$  to 124, respectively.

The shell-model effective interaction sn100pn is made up of  $1g_{7/2}$ ,  $2d_{5/2}$ ,  $2d_{3/2}$ ,  $3s_{1/2}$ ,  $1h_{11/2}$ , orbitals for protons and neutrons in the 50 – 82 model space. The SPEs (in MeV) for neutrons orbitals are  $-10.609$ ,  $-10.289$ ,  $-8.717$ ,  $-8.694$ , and  $-8.815$  corresponding to the  $1g_{7/2}$ ,

$2d_{5/2}$ ,  $2d_{3/2}$ ,  $3s_{1/2}$ , and  $1h_{11/2}$  neutron orbitals, respectively. The SPEs (in MeV) for protons orbitals are  $+0.8072$ ,  $+1.5623$ ,  $+3.3160$ ,  $+3.2238$ , and  $+3.6051$  corresponding to neutron orbitals  $1g_{7/2}$ ,  $2d_{5/2}$ ,  $2d_{3/2}$ ,  $3s_{1/2}$ ,  $1h_{11/2}$ , respectively. The residual two-body interaction starts with a G-matrix derived from the CD-Bonn nucleon-nucleon interaction [35]. This sn100pn interaction is designed from Ref. [34]. We have not applied any truncation where sn100pn interaction is used.

The jj56pnb [37] effective interaction is created for valence space where proton numbers ( $Z$ ) ranging from 50 to 82 and neutron numbers ( $N$ ) ranging from 82 to 126. This interaction is derived from N3LO interaction [36] and the Coulomb interaction part is included in the proton-proton interaction part. The proton orbitals  $1g_{7/2}$ ,  $2d_{5/2}$ ,  $2d_{3/2}$ ,  $3s_{1/2}$ ,  $1h_{11/2}$  have SPEs (in MeV)  $-9.667$ ,  $-8.705$ ,  $-6.959$ ,  $-7.327$ ,  $-6.874$  and neutron orbitals  $1h_{9/2}$ ,  $2f_{7/2}$ ,  $2f_{5/2}$ ,  $3p_{3/2}$ ,  $3p_{1/2}$ ,  $1i_{13/2}$  have  $-0.842$ ,  $-2.4030$ ,  $-0.3980$ ,  $-1.549$ ,  $-1.040$ ,  $+0.2970$ , respectively. Using this interaction we have not used any truncation in our calculations.

### III. RESULTS AND DISCUSSION

In the present manuscript, we have calculated the SM half-lives for higher forbidden unique  $\beta^-$  decay transitions. The ground state to ground state  $Q$  values are adopted from AME2020 [43]. The SM half-lives are calculated for  $g_A^{eff} = 1.0$  and  $g_V = 1.0$  and compared with the scaled half-lives from pnQRPA approach for  $g_A^{eff} = 1.0$  which are extracted from Ref. [14], see Tables I-III.

For mass range  $A = 50 - 62$ , the OBTDs are calculated using gxpfla interaction without truncation. Table I clearly shows that as forbiddenness increases, the half-lives also increase by several orders of magnitude. The half-lives vary from an hour to several years. For example, the SM half-life for  $^{52}\text{Sc}(3^+) \rightarrow ^{52}\text{Ti}(0^+)$  is 54.3 h and for  $^{60}\text{Fe}(0^+) \rightarrow ^{60}\text{Co}(5^+)$  is  $2.2 \times 10^{19}$  year, respectively and these half-lives are also comparable with scaled half-lives from pnQRPA approach. In the case of  $^{58}\text{Co}^*$ , the involved excited isomeric state is represented by an asterisk(\*), similar notation has been used for other isomeric states. For  $^{52}\text{V}$  and  $^{62}\text{Co}^*$ , we see a large difference in the order of half-lives from SM and pnQRPA approach. For  $^{58}\text{Co}^*(5^+) \rightarrow ^{58}\text{Ni}(0^+)$  and  $^{60}\text{Fe}(0^+) \rightarrow ^{60}\text{Co}(5^+)$  transitions, the half-lives are longer as compared to other 4th- FU transitions in the mass range  $A=50-62$  because of small  $Q$ -values involved.

We have employed gwboxg effective interaction for the  $^{84}\text{Se}$  to  $^{104}\text{Rh}^*$ . From  $^{84}\text{Se}$  to  $^{92}\text{Nb}$ , in our SM calculations, we filled  $2p_{1/2}$  neutron orbital to make  $^{68}\text{Ni}$  as a core and there is further one neutron excitation from  $1g_{9/2}$  to  $1g_{7/2}$ ,  $2d_{5/2}$ ,  $2d_{3/2}$ , and  $3s_{1/2}$  orbitals. From  $^{94}\text{Nb}^*$  to  $^{104}\text{Rh}^*$ , we have completely filled the lower orbitals  $2p_{1/2}$ ,  $1g_{9/2}$  to make  $^{78}\text{Ni}$  as a core. For the cases of  $^{84}\text{Se}$ ,  $^{84}\text{Rb}^*$ ,  $^{104}\text{Tc}$  and  $^{104}\text{Rh}^*$ , we obtain a large dif-

TABLE I. Comparison of shell model half-lives for 2nd-, 3rd-, 4th-, 5th-, 6th- and 7th- FU  $\beta^-$  transitions with coupling constants  $g_A^{eff}=1.0$ ,  $g_V=1.0$ , and half-lives using pnQRPA approach with  $g_A^{eff}=1.0$  [14]. The ground-state to ground-state Q value is taken from AME2020 [43]. Here, the  $0^+$  is the ground state of an even-even nucleus and the asterisk (\*) represents the involved isomeric states.

Transition $\beta^-$ Decay	Forbiddenness Kth FU	Q value (keV)	Partial half-life		Interaction
			SM	Ref [14]	
$^{50}\text{Ca}(0^+) \rightarrow ^{50}\text{Sc}(5^+)$	4th FU	4947.9(30)	$2.8 \times 10^5$ yr	$3.3(5) \times 10^5$ yr	gxpfla
$^{50}\text{Sc}(5^+) \rightarrow ^{50}\text{Ti}(0^+)$	4th FU	6894.7(25)	$1.0 \times 10^5$ yr	$1.3(2) \times 10^5$ yr	gxpfla
$^{52}\text{V}(3^+) \rightarrow ^{52}\text{Cr}(0^+)$	2nd FU	3976.48(16)	1.2 yr	$7.3(9) \times 10^3$ yr	gxpfla
$^{52}\text{Ti}(0^+) \rightarrow ^{52}\text{V}(3^+)$	2nd FU	1965.3(28)	$4.0 \times 10^1$ yr	$1.1(20) \times 10^2$ yr	gxpfla
$^{52}\text{Sc}(3^+) \rightarrow ^{52}\text{Ti}(0^+)$	2nd FU	8954 (4)	54.3 h	34.4(5) h	gxpfla
$^{54}\text{V}(3^+) \rightarrow ^{54}\text{Cr}(0^+)$	2nd FU	7037 (11)	24.6 d	9.4(2) d	gxpfla
$^{54}\text{Mn}(3^+) \rightarrow ^{54}\text{Fe}(0^+)$	2nd FU	696.4(11)	$6.5 \times 10^5$ yr	$6.3(9) \times 10^5$ yr	gxpfla
$^{56}\text{Cr}(0^+) \rightarrow ^{56}\text{Mn}(3^+)$	2nd FU	1626.5(6)	$9.5 \times 10^2$ yr	$4.4(60) \times 10^2$ yr	gxpfla
$^{56}\text{Mn}(3^+) \rightarrow ^{56}\text{Fe}(0^+)$	2nd FU	3695.50(21)	4.1 yr	3.9(6) yr	gxpfla
$^{58}\text{Co}^*(5^+) \rightarrow ^{58}\text{Ni}(0^+)$	4th FU	381.6(11)	$2.0 \times 10^{18}$ yr	$1.3(2) \times 10^{18}$ yr	gxpfla
$^{60}\text{Fe}(0^+) \rightarrow ^{60}\text{Co}(5^+)$	4th FU	237(3)	$2.2 \times 10^{19}$ yr	$2.5(4) \times 10^{19}$ yr	gxpfla
$^{60}\text{Co}(5^+) \rightarrow ^{60}\text{Ni}(0^+)$	4th FU	2822.81(21)	$2.4 \times 10^9$ yr	$3.1(5) \times 10^9$ yr	gxpfla
$^{62}\text{Fe}(0^+) \rightarrow ^{62}\text{Co}^*(5^+)$	4th FU	2546(19)	$2.9 \times 10^9$ yr	$1.9(4) \times 10^9$ yr	gxpfla
$^{62}\text{Co}^*(5^+) \rightarrow ^{62}\text{Ni}(0^+)$	4th FU	5322 (19)	$1.1 \times 10^7$ yr	$4.7(6) \times 10^{12}$ yr	gxpfla
$^{84}\text{Se}(0^+) \rightarrow ^{84}\text{Br}^*(6^-)$	5th FU	1835(26)	$8.5 \times 10^{17}$ yr	$2.7(8) \times 10^{19}$ yr	gwbxg
$^{84}\text{Br}^*(6^-) \rightarrow ^{84}\text{Kr}(0^+)$	5th FU	4656(26)	$9.0 \times 10^9$ yr	$1.7(3) \times 10^{10}$ yr	gwbxg
$^{84}\text{Rb}^*(6^-) \rightarrow ^{84}\text{Sr}(0^+)$	5th FU	890.6(23)	$1.1 \times 10^{21}$ yr	$1.7(3) \times 10^{17}$ yr	gwbxg
$^{86}\text{Rb}^*(6^-) \rightarrow ^{86}\text{Sr}(0^+)$	5th FU	1776.10(20)	$4.3 \times 10^{14}$ yr	$3.3(5) \times 10^{14}$ yr	gwbxg
$^{92}\text{Nb}(7^+) \rightarrow ^{92}\text{Mo}(0^+)$	6th FU	355.3(18)	$5.8 \times 10^{28}$ yr	$6.3(1) \times 10^{28}$ yr	gwbxg
$^{94}\text{Nb}^*(3^+) \rightarrow ^{94}\text{Mo}(0^+)$	2nd FU	2045.0(15)	$1.1 \times 10^2$ yr	$1.7(30) \times 10^2$ yr	gwbxg
$^{96}\text{Tc}(7^+) \rightarrow ^{96}\text{Ru}(0^+)$	6th FU	259(5)	$4.3 \times 10^{30}$ yr	$1.7(4) \times 10^{30}$ yr	gwbxg
$^{98}\text{Nb}^*(5^+) \rightarrow ^{98}\text{Mo}(0^+)$	4th FU	4591(5)	$3.0 \times 10^7$ yr	$3.0(5) \times 10^6$ yr	gwbxg
$^{100}\text{Nb}^*(5^+) \rightarrow ^{100}\text{Mo}(0^+)$	4th FU	6402(8)	$4.3 \times 10^4$ yr	$6.9(9) \times 10^4$ yr	gwbxg
$^{104}\text{Mo}(0^+) \rightarrow ^{104}\text{Tc}(3^+)$	2nd FU	2155(24)	$1.6 \times 10^2$ yr	$4.1(6) \times 10^1$ yr	gwbxg
$^{104}\text{Tc}(3^+) \rightarrow ^{104}\text{Ru}(0^+)$	2nd FU	5597(25)	2.3 yr	78.1(10) d	gwbxg
$^{104}\text{Rh}^*(5^+) \rightarrow ^{104}\text{Pd}(0^+)$	4th FU	2435.8(27)	$4.4 \times 10^{11}$ yr	$2.5(4) \times 10^9$ yr	gwbxg
$^{98}\text{Zr}(0^+) \rightarrow ^{98}\text{Nb}^*(5^+)$	4th FU	2243(10)	$8.3 \times 10^8$ yr	$1.7(3) \times 10^9$ yr	G-matrix
$^{100}\text{Zr}(0^+) \rightarrow ^{100}\text{Nb}^*(5^+)$	4th FU	3419(11)	$9.1 \times 10^7$ yr	$3.1(6) \times 10^7$ yr	G-matrix

ference in the half-lives between SM and pnQRPA approaches.

We have performed SM calculations without any truncations, using the G-matrix effective interaction for  $^{98}\text{Zr}$  to  $^{124}\text{Cd}$ . For most of the transitions, we obtain larger SM half-lives compared to the scaled half-lives from the pnQRPA. However, in the cases of  $^{98}\text{Zr}(0^+) \rightarrow ^{98}\text{Nb}^*(5^+)$  and  $^{122}\text{Cd}(0^+) \rightarrow ^{122}\text{In}^*(5^+)$  transitions, the SM half-lives are shorter than the scaled pnQRPA half-lives.

In the Indium chain, we have performed the SM calculations using snet effective interaction. Due to large dimensions, we have restricted the neutron orbitals. For  $^{114}\text{In}$  and  $^{116}\text{In}$  we have applied a truncation of  $\nu h_{11/2}^{(0-2)}$ , for  $^{118}\text{In}$  and  $^{120}\text{In}$ , a truncation of  $\nu h_{11/2}^{(0-4)}$  and for  $^{122}\text{In}$  and  $^{124}\text{In}$ , a truncation of  $\nu h_{11/2}^{(0-6)}$ , respectively. Here, all the decay transitions are from the isomeric excited states of odd-odd nuclei to g.s. of an even-even nuclei. The SM half-lives for all In isotopes are shorter than the scaled pnQRPA half-lives except for  $^{114}\text{In}^*(5^+) \rightarrow ^{114}\text{Sn}(0^+)$  transition.

We have performed the SM calculations using sn100pn

effective interaction for the decay transitions in the cases of  $^{126-130}\text{Sn}$ ,  $^{120-132}\text{Sb}$ ,  $^{134}\text{Te}$ ,  $^{130,134}\text{I}$ ,  $^{134,136}\text{Cs}$ , and  $^{138}\text{La}$  nuclei. We have not employed any truncation except for  $^{120,122}\text{Sb}$ . A minimum of 6-8 neutrons in the  $1g_{7/2}$  orbital ( $\nu g_{7/2}^{(6-8)}$ ) are restricted in the cases for  $^{120,122}\text{Sb}$ . The SM half-lives are longer in most cases, with a few in reasonable agreement with the scaled pnQRPA half-lives.

For  $^{136}\text{Te}$  and  $^{138}\text{Xe}$ , we have employed the SM calculations using jj56pnb effective interaction without any truncation. For these nuclei, we are getting a difference of one order of magnitude in their half-lives between SM and pnQRPA approach.

In Table II B, we compare SM half-lives with the measured half-lives or lower limits for the transitions  $^{40}\text{K}(4^-) \rightarrow ^{40}\text{Ca}(0^+)$ ,  $^{48}\text{Ca}(0^+) \rightarrow ^{48}\text{Sc}(5^+)$ ,  $^{96}\text{Zr}(0^+) \rightarrow ^{96}\text{Nb}(5^+)$  and  $^{138}\text{La}(5^+) \rightarrow ^{138}\text{Ce}(2^+)$ . A detailed discussion and comparison of the SM half-lives with the experimental half-lives for these transitions is reported below.

$^{40}\text{K}(4^-) \rightarrow ^{40}\text{Ca}(0^+)$ : The  $^{40}\text{K}$  is a naturally occurring nucleus and can decay through the  $\beta^-$ ,  $\beta^+$ , and EC

TABLE II. Same as Table I.

Transition $\beta^-$ Decay	Forbiddenness Kth FU	Q value (keV)	Partial half-life		Interaction
			SM	Ref. [14]	
$^{118}\text{Cd}(0^+) \rightarrow ^{118}\text{In}^*(5^+)$	4th FU	527(21)	$2.5 \times 10^{16}$ yr	$1.8(5) \times 10^{16}$ yr	G-matrix
$^{118}\text{Cd}(0^+) \rightarrow ^{118}\text{In}^*(8^-)$	7th FU	527(21)	$8.6 \times 10^{33}$ yr	$3.1(1\text{mag}) \times 10^{32}$ yr	G-matrix
$^{120}\text{Cd}(0^+) \rightarrow ^{120}\text{In}^*(5^+)$	4th FU	1770(40)	$7.0 \times 10^{10}$ yr	$3.8(8) \times 10^{10}$ yr	G-matrix
$^{120}\text{Cd}(0^+) \rightarrow ^{120}\text{In}^*(8^-)$	7th FU	1770(40)	$5.5 \times 10^{24}$ yr	$2.2(3) \times 10^{22}$ yr	G-matrix
$^{120}\text{Pd}(0^+) \rightarrow ^{120}\text{Ag}^*(6^-)$	5th FU	5372(5)	$1.4 \times 10^{10}$ yr	$4.4(7) \times 10^8$ yr	G-matrix
$^{120}\text{Pd}(0^+) \rightarrow ^{120}\text{Ag}(3^+)$	2nd FU	5372(5)	30.4 d	8.8(6) d	G-matrix
$^{120}\text{Ag}(3^+) \rightarrow ^{120}\text{Cd}(0^+)$	2nd FU	8306(6)	6.4 d	4.5(8) d	G-matrix
$^{120}\text{Ag}^*(6^-) \rightarrow ^{120}\text{Cd}(0^+)$	5th FU	8306(6)	$9.0 \times 10^7$ yr	$2.2(4) \times 10^6$ yr	G-matrix
$^{122}\text{Cd}(0^+) \rightarrow ^{122}\text{In}^*(8^-)$	7th FU	2960(50)	$8.6 \times 10^{19}$ yr	$2.0(7) \times 10^{19}$ yr	G-matrix
$^{122}\text{Cd}(0^+) \rightarrow ^{122}\text{In}^*(5^+)$	4th FU	2960(50)	$3.2 \times 10^7$ yr	$2.0(4) \times 10^8$ yr	G-matrix
$^{124}\text{Cd}(0^+) \rightarrow ^{124}\text{In}^*(8^-)$	7th FU	4170(30)	$1.8 \times 10^{17}$ yr	$9.4(2) \times 10^{15}$ yr	G-matrix
$^{114}\text{In}^*(5^+) \rightarrow ^{114}\text{Sn}(0^+)$	4th FU	1989.9(3)	$2.6 \times 10^{12}$ yr	$9.4(2) \times 10^9$ yr	snet
$^{116}\text{In}^*(5^+) \rightarrow ^{116}\text{Sn}(0^+)$	4th FU	3276.22(24)	$3.8 \times 10^9$ yr	$1.7(3) \times 10^{13}$ yr	snet
$^{116}\text{In}^*(8^-) \rightarrow ^{116}\text{Sn}(0^+)$	7th FU	3276.22(24)	$5.4 \times 10^{20}$ yr	$1.4(2) \times 10^{30}$ yr	snet
$^{118}\text{In}^*(5^+) \rightarrow ^{118}\text{Sn}(0^+)$	4th FU	4425(8)	$1.3 \times 10^8$ yr	$1.7(3) \times 10^{12}$ yr	snet
$^{118}\text{In}^*(8^-) \rightarrow ^{118}\text{Sn}(0^+)$	7th FU	4425(8)	$3.1 \times 10^{18}$ yr	$4.2(5) \times 10^{20}$ yr	snet
$^{120}\text{In}^*(5^+) \rightarrow ^{120}\text{Sn}(0^+)$	4th FU	5370(40)	$1.2 \times 10^7$ yr	$4.0(6) \times 10^{17}$ yr	snet
$^{122}\text{In}^*(5^+) \rightarrow ^{122}\text{Sn}(0^+)$	4th FU	6370(50)	$2.1 \times 10^6$ yr	$1.1(2) \times 10^{14}$ yr	snet
$^{122}\text{In}^*(8^-) \rightarrow ^{122}\text{Sn}(0^+)$	7th FU	6370(50)	$4.1 \times 10^{15}$ yr	$4.7(2) \times 10^{18}$ yr	snet
$^{124}\text{In}^*(8^-) \rightarrow ^{124}\text{Sn}(0^+)$	7th FU	7360(30)	$6.4 \times 10^{14}$ yr	$5.3(8) \times 10^{18}$ yr	snet
$^{126}\text{Sn}(0^+) \rightarrow ^{126}\text{Sb}^*(5^+)$	4th FU	378(30)	$2.6 \times 10^{18}$ yr	$4.7(1\text{mag}) \times 10^{18}$ yr	sn100pn
$^{126}\text{Sn}(0^+) \rightarrow ^{126}\text{Sb}(8^-)$	7th FU	378(30)	$3.7 \times 10^{33}$ yr	$2.3(4) \times 10^{15}$ yr	sn100pn
$^{128}\text{Sn}(0^+) \rightarrow ^{128}\text{Sb}^*(5^+)$	4th FU	1268(13)	$1.2 \times 10^{13}$ yr	$2.8(4) \times 10^{13}$ yr	sn100pn
$^{128}\text{Sn}(0^+) \rightarrow ^{128}\text{Sb}(8^-)$	7th FU	1268(13)	$1.1 \times 10^{26}$ yr	$1.4(3) \times 10^{23}$ yr	sn100pn
$^{130}\text{Sn}(0^+) \rightarrow ^{130}\text{Sb}(8^-)$	7th FU	2153(14)	$2.3 \times 10^{22}$ yr	$3.1(5) \times 10^{19}$ yr	sn100pn
$^{120}\text{Sb}^*(8^-) \rightarrow ^{120}\text{Te}(0^+)$	7th FU	945(7)	$8.3 \times 10^{29}$ yr	$4.7(1) \times 10^{26}$ yr	sn100pn
$^{122}\text{Sb}^*(8^-) \rightarrow ^{122}\text{Te}(0^+)$	7th FU	1979.1(21)	$2.8 \times 10^{24}$ yr	$4.7(6) \times 10^{21}$ yr	sn100pn
$^{124}\text{Sb}^*(5^+) \rightarrow ^{124}\text{Te}(0^+)$	4th FU	2905.07(13)	$9.0 \times 10^{10}$ yr	$1.9(3) \times 10^{12}$ yr	sn100pn
$^{124}\text{Sb}^*(8^-) \rightarrow ^{124}\text{Te}(0^+)$	7th FU	2905.07(13)	$1.8 \times 10^{22}$ yr	$3.4(5) \times 10^{19}$ yr	sn100pn
$^{126}\text{Sb}^*(5^+) \rightarrow ^{126}\text{Te}(0^+)$	4th FU	3670(30)	$6.7 \times 10^9$ yr	$1.1(2) \times 10^{11}$ yr	sn100pn

TABLE III. Same as Table I.

Transition $\beta^-$ Decay	Forbiddenness Kth FU	Q value (keV)	Partial half-life		Interaction
			SM	Ref. [14]	
$^{126}\text{Sb}(8^-) \rightarrow ^{126}\text{Te}(0^+)$	7th FU	3670(30)	$5.0 \times 10^{20}$ yr	$1.1(2) \times 10^{18}$ yr	sn100pn
$^{128}\text{Sb}^*(5^+) \rightarrow ^{128}\text{Te}(0^+)$	4th FU	4364(19)	$1.0 \times 10^9$ yr	$1.6(2) \times 10^{10}$ yr	sn100pn
$^{130}\text{Sb}(8^-) \rightarrow ^{130}\text{Te}(0^+)$	7th FU	5067(14)	$4.0 \times 10^{18}$ yr	$9.4(2) \times 10^{15}$ yr	sn100pn
$^{132}\text{Sb}(8^-) \rightarrow ^{132}\text{Te}(0^+)$	7th FU	5553(4)	$1.2 \times 10^{18}$ yr	$4.4(6) \times 10^{15}$ yr	sn100pn
$^{134}\text{Te}(0^+) \rightarrow ^{134}\text{I}^*(8^-)$	7th FU	1510(5)	$7.6 \times 10^{26}$ yr	$3.1(5) \times 10^{23}$ yr	sn100pn
$^{130}\text{I}(5^+) \rightarrow ^{130}\text{Xe}(0^+)$	4th FU	2944(3)	$1.5 \times 10^{11}$ yr	$7.8(1) \times 10^{11}$ yr	sn100pn
$^{134}\text{I}^*(8^-) \rightarrow ^{134}\text{Xe}(0^+)$	7th FU	4082(5)	$1.7 \times 10^{20}$ yr	$1.1(2) \times 10^{17}$ yr	sn100pn
$^{134}\text{Cs}^*(8^-) \rightarrow ^{134}\text{Ba}(0^+)$	7th FU	2058.84(25)	$5.9 \times 10^{24}$ yr	$3.9(5) \times 10^{21}$ yr	sn100pn
$^{136}\text{Cs}(5^+) \rightarrow ^{136}\text{Ba}(0^+)$	4th FU	2548.2(19)	$4.8 \times 10^{11}$ yr	$7.8(1) \times 10^{11}$ yr	sn100pn
$^{136}\text{Cs}^*(8^-) \rightarrow ^{136}\text{Ba}(0^+)$	7th FU	2548.2(19)	$5.0 \times 10^{23}$ yr	$3.1(5) \times 10^{19}$ yr	sn100pn
$^{138}\text{La}(5^+) \rightarrow ^{138}\text{Ce}(0^+)$	4th FU	1052.42(41)	$6.2 \times 10^{15}$ yr	$1.4(3) \times 10^{16}$ yr	sn100pn
$^{136}\text{Te}(0^+) \rightarrow ^{136}\text{I}^*(6^-)$	5th FU	5120(14)	$2.0 \times 10^8$ yr	$2.3(5) \times 10^9$ yr	jj56pnb
$^{138}\text{Xe}(0^+) \rightarrow ^{138}\text{Cs}^*(6^-)$	5th FU	2915(10)	$3.0 \times 10^{12}$ yr	$1.3(3) \times 10^{11}$ yr	jj56pnb

channels. The  $^{40}\text{K}$  isotope is important for geochronological applications. The partial half-life for  $\beta^-$  channel is  $1.398(3) \times 10^9$  yr with branching ratio 89.28(13)% for the corresponding transition [44]. The recent measurements have been made for the spectral shape of the  $\beta$ -spectra [48]. For this transition, the OBTDs are obtained from

the SM using the 2p-2h truncation corresponding to excitation from  $sd$  to  $pf$  shell to get  $4^-$  state of  $^{40}\text{K}$  and  $0^+$  of  $^{40}\text{Ca}$  using  $sd$ - $pf$ - $\mu$  interaction. The shell model half-life is  $9.2 \times 10^8$  yr for this transition with the values  $g_A^{eff} = 1.0$  and  $g_V = 1.0$ . The variation of the shell-

TABLE IV. Comparison of shell model half-lives for  $\beta^-$  transitions with the coupling constants  $g_A^{eff}=1.0$ ,  $g_V=1.0$ , and the measured half-lives (or lower limits). The ground-state to ground-state Q value is taken from AME2020 [43].

Transition	Forbiddenness	Q value (keV)	Partial half-life (yr)		Interaction
			Experimental	SM	
$^{40}\text{K}(4^-) \rightarrow ^{40}\text{Ca}(0^+)$	3rd FU	1310.91(6)	$1.398(3) \times 10^9$ [44, 45]	$9.2 \times 10^8$	sdpf-mu
$^{48}\text{Ca}(0^+) \rightarrow ^{48}\text{Sc}(5^+)$	4th FU	279(5)	$> 2.5 \times 10^{20}$ [46]	$5.1 \times 10^{20}$	gxpfla
$^{96}\text{Zr}(0^+) \rightarrow ^{96}\text{Nb}(5^+)$	4th FU	163.97(10)	$> 2.4 \times 10^{19}$ [47]	$1.3 \times 10^{20}$	gwbxg
$^{138}\text{La}(5^+) \rightarrow ^{138}\text{Ce}(2^+)$	2nd FU	1052.5(4)	$2.97(3) \times 10^{11}$ [44, 45]	$7.7 \times 10^{10}$	sn100pn

model partial half-life with the different  $g_A^{eff}$  values is shown in Fig. 1.

$^{48}\text{Ca}(0^+) \rightarrow ^{48}\text{Sc}(5^+)$ : The doubly magic nucleus  $^{48}\text{Ca}$  is unstable against a single beta decay. The  $^{48}\text{Ca}$  ( $0^+$ ) can decay to  $4^+$ ,  $5^+$ ,  $6^+$  states of the daughter nucleus  $^{48}\text{Sc}$  which is followed by a large change in angular momentum along with a small Q value. The decay to  $4^+$  and  $6^+$  states are FNU decay and to  $5^+$  state is a FU decay. Previously, Aunola et al. and Haaranen et al. estimated partial half-lives of  $1.1_{-0.6}^{+0.8} \times 10^{21}$  yr [49] and  $5.2_{-1.3}^{+1.7} \times 10^{20} g_A^{-2}$  yr [50], respectively. For the  $^{48}\text{Ca}$  case, there is a competition between single  $\beta^-$  and  $\beta\beta^-$  decay channel with the observed half life for  $\beta\beta^-$  decay channel is  $6.4 \times 10^{19}$  yr [51]. In the present calculations, the SM half-life corresponding to a single  $\beta^-$  decay is  $5.0 \times 10^{20}$  yr for  $g_A^{eff} = 1.0$  and  $g_V = 1.0$  and the experimental limit for the half-life is greater than  $2.5 \times 10^{20}$  yr given in Ref. [46].

$^{96}\text{Zr}(0^+) \rightarrow ^{96}\text{Nb}(5^+)$ : This case is similar to previous  $^{48}\text{Ca}$  case. The  $0^+$  g.s. can decay to  $4^+$ ,  $5^+$  and  $6^+$  states of daughter nucleus  $^{96}\text{Nb}$  and the most likely branch is 4th- FU decay. The higher forbiddenness 4th- FU decay along with the low Q-value have a longer half-life as compared to the double beta decay channel. The recently measured lower limit of experimental single beta decay half-life is greater than  $2.4 \times 10^{19}$  yr [47]. Previously, calculated shell-model half-life was  $(11g_A^{-2}) \times 10^{19}$  yr [52] and QRPA half-life was  $2.4 \times 10^{20}$  yr [53]. In the present work, the calculated shell model half-life with  $g_A^{eff} = 1.0$  and  $g_V = 1.0$  (g.s. to g.s. Q value 163.97(0.10) keV) is  $1.3 \times 10^{20}$  yr.

$^{138}\text{La}(5^+) \rightarrow ^{138}\text{Ce}(2^+)$ :  $^{138}\text{La}$  is a naturally occurring nucleus with half-life of  $1.02(1) \times 10^{11}$  yr [54]. The branching ratio for 2nd- FU  $\beta^-$  decay  $^{138}\text{La}(5^+) \rightarrow ^{138}\text{Ce}^*(2^+)$  is 34.5% and the partial half-life for the corresponding transition is  $2.97(3) \times 10^{11}$  yr. The SM calculations predict the half-life value  $7.7 \times 10^{10}$  yr with  $g_A^{eff} = 1.0$  and  $g_V=1.0$ . The variation of shell-model results of partial half-life with the  $g_A^{eff}$  values is shown in Fig. 1.

#### IV. CONCLUSION

In the present work, we have performed the SM calculations for higher  $\beta^-$  decay transitions including 2nd-

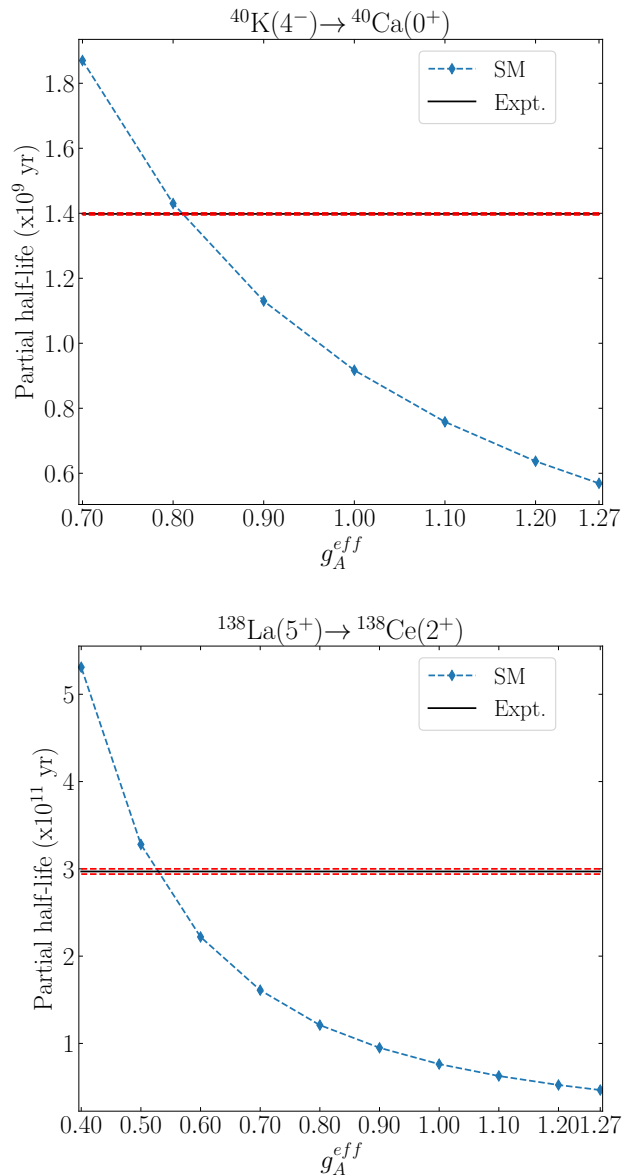


FIG. 1. The variation of shell model partial half-life with  $g_V = 1.0$  and different  $g_A^{eff}$  values. The vertical dashed lines (red in colour) are the error value of the experimental partial half-life.

, 3rd-, 4th-, 5th-, 6th- and 7th- FU, for nuclei in mass range  $A=40-138$ . We have employed the effective interactions `sdpf-mu`, `gxpfla`, `gwbxg`, `G-matrix`, `snet`, `sn100pn`, and `jj56pn` to obtain the OBTDs. Further, the OBTDs have been used to calculate the partial half-lives within the framework of  $\beta$ -decay theory. The present manuscript is focused on those higher FU decay transitions for which experimental data is unavailable except for the 3rd-FU  $^{40}\text{K}(4^-) \rightarrow ^{40}\text{Ca}(0^+)$ , 4th- FU,  $^{48}\text{Ca}(0^+) \rightarrow ^{48}\text{Sc}(5^+)$ , 4th- FU  $^{96}\text{Zr}(0^+) \rightarrow ^{96}\text{Nb}(5^+)$  and 2nd- FU  $^{138}\text{La}(5^+) \rightarrow ^{138}\text{Ce}(2^+)$  transitions. For these transitions, the measured half-life or its lower limit is available. The calculations are performed with  $g_A^{eff}=1.0$  and  $g_V=1.0$  and results are compared with the expected

half-lives from pnQRPA approach at  $g_A^{eff}=1.0$ . The variation in half-lives between the two approaches is due to the use of different nuclear structure formalism involved. The present SM study will be useful to compare upcoming experimental data for half-lives of these higher forbidden  $\beta^-$  decay transitions.

## ACKNOWLEDGEMENT

This work is supported by a research grant from SERB (India), CRG/2022/005167. We also acknowledge the National Supercomputing Mission (NSM) for providing computing resources of ‘PARAM Ganga’ at the Indian Institute of Technology Roorkee. We would also like to thank Anil Kumar for the useful discussion.

- 
- [1] K. Langanke and G. Martínez-Pinedo, “Nuclear weak-interaction processes in stars”, *Rev. Mod. Phys.* **75**, 819 (2003).
- [2] T. Suzuki, “Nuclear weak rates and nuclear weak processes in stars”, *Progress in Particle and Nuclear Physics* **126**, 103974 (2022).
- [3] E. Caurier, K. Langanke, G. Martínez-Pinedo and F. Nowacki, “Shell-model calculations of stellar weak interaction rates. I. Gamow-Teller distributions and spectra of nuclei in the mass range  $A=45-65$ ”, *Nucl. Phys. A* **653**, 439 (1999).
- [4] K. Langanke and G. Martínez-Pinedo, “Shell-model calculations of stellar weak interaction rates: Weak rates for nuclei in the mass range  $A=45-65$  in supernovae environments”, *Nucl. Phys. A* **673**, 481 (2000).
- [5] H. Schatz et al., “Strong neutrino cooling by cycles of electron capture and  $\beta^-$  decay in neutron star crusts”, *Nature* **505**, 62 (2014).
- [6] T. Suzuki, H. Toki, and K. Nomoto, “Electron-capture and  $\beta$ -decay rates for sd-shell nuclei in stellar environments relevant to high-density O-Ne-Mg cores”, *The Astrophysical Journal*, **817**, 163 (2016).
- [7] A. Saxena, P.C. Srivastava and T. Suzuki, “Ab initio calculations of Gamow-Teller strengths in the *sd* shell nuclei”, *Phys. Rev. C* **97**, 024310 (2018).
- [8] A. Kumar, N. Shimizu, Y. Utsuno, C. Yuan, and P. C. Srivastava, “Large-scale shell model study of  $\beta^-$ -decay properties of  $N=126, 125$  nuclei: Role of Gamow-Teller and first-forbidden transitions in the half-lives”, *Phys. Rev. C* **109**, 064319 (2024).
- [9] S. Sharma, P. C. Srivastava, A. Kumar, and T. Suzuki, “Shell-model description for the properties of the forbidden  $\beta$ -decay in the region “northeast” of  $^{208}\text{Pb}$ ”, *Phys. Rev. C* **106**, 024333 (2022).
- [10] S. Sharma, P. C. Srivastava, A. Kumar, T. Suzuki, C. Yuan, and N. Shimizu, “Shell-model study for allowed and forbidden  $\beta$ -decay properties in the mass region “south” of  $^{208}\text{Pb}$ ”, *Phys. Rev. C* **110**, 024320 (2024).
- [11] J. T. Suhonen, “Value of the Axial-Vector Coupling Strength in  $\beta$  and  $\beta\beta$  Decays: A Review”, *Front. Phys.* **5**, 55 (2017).
- [12] J. Suhonen, *From Nucleons to Nucleus: Concept of Microscopic Nuclear Theory*, (Springer, Berlin 2007).
- [13] H. Behrens and W. Bühring, *Electron Radial Wave Functions and Nuclear Beta-Decay* (Clarendon Press, 1982).
- [14] J. Kostensalo, and J. Suhonen, “Spin-multipole nuclear matrix elements in the *pn* quasiparticle random-phase approximation: Implications for  $\beta$  and  $\beta\beta$  half-lives”, *Phys. Rev. C* **95**, 014322 (2017).
- [15] H. Ejiri, N. Soukouti and J. Suhonen, “Spin-dipole nuclear matrix elements for double beta decays and astro-neutrinos”, *Phys. Lett. B* **729**, 27 (2014).
- [16] H. Ejiri and J. Suhonen, “GT neutrino-nuclear responses for double beta decays and astro neutrinos”, *J. Phys. G: Nucl. Part. Phys.* **42**, 055201 (2015).
- [17] J. Kostensalo and J. Suhonen, “ $g_A$ -driven shapes of electron spectra of forbidden  $\beta$  decays in the nuclear shell-model”, *Phys. Rev. C* **96**, 024317 (2017).
- [18] A. Kumar, P. C. Srivastava, and J. Suhonen, “Second-forbidden nonunique  $\beta^-$  decays of  $^{59,60}\text{Fe}$ : possible candidates for  $g_A$  sensitive electron spectral-shape measurements”, *Eur. Phys. J. A* **57**, 225(2021).
- [19] M. Haaranen, P. C. Srivastava, and J. Suhonen “Forbidden non-unique  $\beta$  decays and effective values of weak coupling constants”, *Phys. Rev. C* **93**, 034308 (2016).
- [20] M. Haaranen, J. Kotila, and J. Suhonen, “Spectrum-shape method and the next-to-leading-order terms of the  $\beta$ -decay shape factor”, *Phys. Rev. C* **95**, 024327 (2017).
- [21] M. T. Mustonen, M. Aunola, and J. Suhonen, “Theoretical description of the fourth-forbidden non-unique  $\beta$  decays of  $^{113}\text{Cd}$  and  $^{115}\text{In}$ ”, *Phys. Rev. C* **73**, 054301 (2006); Erratum *Phys. Rev. C* **76**, 019901 (2007).
- [22] H. F. Schopper, *Weak Interaction and Nuclear Beta Decay* (North-Holland, Amsterdam, 1966).
- [23] C. Patrignani and Particle Data Group, “Review of Particle Physics”, *Chinese Phys. C* **40**, 100001 (2016).
- [24] A. Kumar, P. C. Srivastava, J. Kostensalo and J. Suhonen, “Second-forbidden nonunique  $\beta^-$  decays of  $^{24}\text{Na}$  and  $^{36}\text{Cl}$  assessed by the nuclear shell-model”, *Phys. Rev. C* **101**, 064304 (2020).
- [25] N. Shimizu, T. Mizusaki, Y. Utsuno and Y. Tsunoda, “Thick-restart block Lanczos method for large-scale shell-model calculations”, *Comput. Phys. Commun.* **244**,

- 372–384 (2019).
- [26] B. A. Brown and W. D. M. Rae, The shell-model code NuShellX@MSU, *Nucl. Data Sheets* **120**, 115(2014).
- [27] Y. Utsuno, T. Otsuka, B. A. Brown, M. Honma, T. Mizusaki, and N. Shimizu “Shape transitions in exotic Si and S isotopes and tensor-force-driven Jahn-Teller effect”, *Phys. Rev. C* **86**, 051301(R) (2012).
- [28] M. Honma, T. Otsuka, B. A. Brown, and T. Mizusaki, “Shell-model description of neutron-rich pf-shell nuclei with a new effective interaction GXPF 1”, *Eur. Phys. J. A* **25**, suppl 1, 499 (2005).
- [29] Z. Ren et al., “Reinvestigation of the level structures of the  $N = 49$  isotones  $^{89}\text{Zr}$  and  $^{91}\text{Mo}$ ”, *Phys RevC* **106**, 024323(2022).
- [30] P. Dey et al., “Experimental investigation of high-spin states in  $^{90}\text{Zr}$ ”, *Phys RevC* **105**, 044307(2022).
- [31] N. Boelaert, N. Smirnova, K. Heyde, and J. Jolie, “Shell model description of the low-lying states of the neutron deficient Cd isotopes” *Phys RevC* **75**, 014316 (2007).
- [32] A. Hosaka, et al., “G-matrix effective interaction with the paris potential”, *Nucl. Phys. A* **71**, 444 (1986).
- [33] B.A. Brown, et al., “Gamow-Teller strength in the region of  $^{100}\text{Sn}$ ”, *Phys. Rev. C* **50**, 2270(R) (1994).
- [34] B. A. Brown, N. J. Stone, J. R. Stone, I. S. Towner, and M. Hjorth-Jensen, “Magnetic moments of the  $2_1^+$  states around  $^{132}\text{Sn}$ ”, *Phys RevC* **71**, 044317 (2005).
- [35] R. Machleidt, F. Sammarruca, and Y. Song, “Nonlocal nature of the nuclear force and its impact on nuclear structure”, *Phys. Rev. C* **53** R1483(R) (1996).
- [36] D. R. Entem, and R. Machleidt, “ Accurate charge-dependent nucleon-nucleon potential at fourth order of chiral perturbation theory”, *Phys. Rev. C* **68**, 041001(R) (2003).
- [37] B. A. Brown, unpublished.
- [38] A. Hosaka, K.-I. Kubo and H. Toki, “G-matrix effective interaction with the paris potential”, *Nucl. Phys. A* **444**, 76 (1985).
- [39] X. Ji and B. H. Wildenthal, “Effective interaction for  $N=50$  isotones”, *Phys. Rev. C* **37**, 1256 (1988).
- [40] D. H. Gloeckner, “Shell-model systematics of the zirconium and niobium isotopes ”, *Nucl. Phys. A* **253**, 301 (1975).
- [41] F. J. D. Serduke, R. D. Lawson, and D. H. Gloeckner, “ Shell-model study of the  $N = 49$  isotones”, *Nucl.Phys. A* **256**, 45 (1976).
- [42] R. Machleidt, “High-precision, charge-dependent Bonn nucleon-nucleon potential”, *Phys Rev C* **63**, 024001 (2001).
- [43] M. Wang, W. J. Huang, F. G. Kondev, G. Audi and S. Naimi, “The AME 2020 atomic mass evaluation (II). Tables, graphs and references” *Chin. Phys. C* **45**(3), 030003(2021).
- [44] P. Belli, R. Bernabei, F. A. Danevich, et al., “Experimental searches for rare alpha and beta decays”, *Eur. Phys. J. A* **55**, 140 (2019).
- [45] M. Redshaw, “Precise Q value determinations for forbidden and low energy  $\beta$ -decays using Penning trap mass spectrometry”, *Eur. Phys. J. A* **59**, 18 (2023).
- [46] A. Bakalyarov et al., “Improved limits on  $\beta^-$  and  $\beta\beta^-$  decays of  $^{48}\text{Ca}$ ”, *JETP Lett.* **76**, 545 (2002).
- [47] S. W. Finch, and W. Tornow, “Search for the  $\beta$  decay of  $^{96}\text{Zr}$ ”, *Nucl. Instrum. Methods A* **806**, 70-74(2016).
- [48] A. G. Carles, and K. Kossert, “Management of the shape-factor functions of the long-lived radionuclides  $^{87}\text{Rb}$ ,  $^{40}\text{K}$  and  $^{10}\text{Be}$ ”, *Nucl. Instrum. Methods Phys. Res.* **572**, 760-767(2007).
- [49] M. Aunola, J. Suhonen and T. Siiskonen, “Shell-model study of the highly forbidden beta decay  $^{48}\text{Ca} \rightarrow ^{48}\text{Sc}$ ”, *Europhys. Lett.* **46**, 577 (1999).
- [50] M. Haaranen, M. Horoi, and J. Suhonen, “Shell-model study of the 4th- and 6th-forbidden  $\beta$ -decay branches of  $^{48}\text{Ca}$ ”, *Phys. Rev. C* **89**, 034315 (2014).
- [51] R. Arnold et al., “Measurement of the double-beta decay half-life and search for the neutrinoless double-beta decay of  $^{48}\text{Ca}$  with the NEMO-3 detector”, *Phys. Rev. D* **93**, 112008 (2016).
- [52] M. Alanssari et al., “Single and Double Beta-Decay Q Values among the Triplet  $^{96}\text{Zr}$ ,  $^{96}\text{Nb}$ , and  $^{96}\text{Mo}$ ”, *Phys. Rev. Lett.* **116**, 072501 (2016).
- [53] H Heiskanen, M. T. Mustonen and J. Suhonen, “ Theoretical half-life for beta decay of  $^{96}\text{Zr}$ ”, *J. Phys. G: Nucl. and Part. Phys.* **34**, 837 (2007).
- [54] G. Audi G. et al., “The NUBASE2016 evaluation of nuclear properties”, *Chin. Phys. C* **41**, 030001(2017).